Unimolecular Reaction Rate Constants of NO_2 Just above D_0

I. Bezel, D. Stolyarov, and C. Wittig*

Department of Chemistry, University of Southern California, Los Angeles, California 90089

Received: July 26, 1999; In Final Form: August 26, 1999

Photoinitiated unimolecular decomposition on a barrierless potential energy surface (PES) has been studied for the reaction $NO_2 \rightarrow O(^3P_2) + NO(X^2\Pi_{1/2}, v = 0)$ for excess energies up to approximately 17 cm^{-1} above the dissociation threshold (i.e., D_0 for nonrotating molecules) by using expansion-cooled samples and the time-resolved pump−probe technique. To examine the threshold region with enough energy resolution to discern abrupt changes in the rate constant, should they occur, a pump−probe cross-correlation temporal width of ∼25 ps and a pump line width ≤2 cm^{-1} has been used. These are the first direct observations of the reaction rate constants in this energy regime. The rate constant was found to increase by an order of magnitude, varying from $\sim 2 \times 10^{10}$ s^{-1} to $\geq 10^{11}$ s^{-1}, the latter being a rough lower bound imposed by the experimental arrangement. The rate constant does not display the energy dependence predicted by using phase space theory, at least in detail. Rather, it appears to reflect the highly complex nature of the levels and the multiple PESs that are believed to be responsible for the anomalously high vibronic level density which has been observed just below D_0. These results bridge the gap between spectroscopic studies which have been carried out at energies just above D_0 and ultrafast experiments which have measured rate constants in this energy region with pump laser spectral widths of ∼30 cm^{-1}.

I. Introduction

Measurements of NO_2 unimolecular decomposition rate constants at energies just above reaction threshold (i.e., D_0 for nonrotating molecules) can be used as an indirect probe of the participating potential energy surfaces (PESs) at large bond extensions. In this regime, the mean value of the resonance widths, $\langle \Gamma_i \rangle$, is believed to be the same as the unimolecular decomposition rate constant, k, which can be calculated by using statistical models such as phase space theory (PST) and Rice, Ramsperger, Kassel, and Marcus (RRKM) theory, i.e., $k = \langle \Gamma_i \rangle$.[1] However, upon closer inspection, the connection between the reactive resonances (Γ_i) and the various versions of transition state theory (TST) applied to barrierless unimolecular reactions is rather subtle in the threshold regime. For example, at energies where a reactive channel just opens, the de Broglie wavelength for relative translational motion in this channel is much larger than the size of the molecule, so a neatly defined transition state (TS) region is not meaningful. Lore has it that in such a case the transition state lies at infinity, which is also a curious notion. (Were the TS at infinity, it would take forever for the products to get past the TS, whereas in the statistical theory the rate constant for an open channel is given by $1/h\rho$ times the degeneracy of the open channel, where ρ is the density of states and h is Planck's constant.)

The nature of reactive resonances in unimolecular decomposition has been studied both theoretically and experimentally. Theoretical studies which model specific molecular systems have relied heavily on ground state PESs, and threshold regimes have not been emphasized.[2−6] This work has resulted in an improved, albeit largely qualitative, understanding, including some clarification and quantification of the relationships between conceptually straightforward dynamics calculations of good accuracy (i.e., using the best currently available PESs)[7−10] and the more abstract mathematical formalisms that deal with level statistics.[11,12] However, such studies are not very germane to the threshold regimes of barrierless reactions.

Just above D_0, reactive resonances of NO_2 have been observed by using expansion-cooled samples and several complementary spectroscopic techniques.[13−20] In all cases, the spectra are congested, i.e., not a single isolated transition has ever been observed, even with very cold (i.e., ∼1 K) samples. This is interesting in itself. TST predicts that for a set of good quantum numbers (i.e., total angular momentum and its projection on a space-fixed axis) the ratio of the average separation between adjacent resonances and the average resonance width is $2\pi/W$,[21] where W is the number of open channels including degeneracies. For NO_2 decomposing to the lowest product electronic states, i.e., $O(^3P_2) + NO(X^2\Pi_{1/2})$, the first open channel (i.e., corresponding to the lowest NO rotational level, $J_{NO} = 1/2$) has degeneracies of 4 and 8 for $J_{NO_2} = 1/2$ and 3/2, respectively, as discussed in the Appendix. Note that $J_{NO_2} =$ 1/2 and 3/2 are both optically accessible from $J_{NO_2} = 1/2$. Thus, it is not surprising that for the lowest open channel isolated reson ances are not observed. This underscores the point that, in nearly all cases, unimolecular reactions involve *overlapping* resonances.

The line width analyses of Miyawaki et al.[15] and Abel et al.[17] confirm the fact that the rate constants fluctuate, and they suggest an average threshold rate constant of $\sim 2 \times 10^{10}$ s^{-1} for the first open channel. As mentioned above, the first open channel corresponds to the energy region over which NO is formed in its ground rotational level. The second channel is believed to open at approximately the energy of the first excited rotational level (i.e., 5 cm^{-1}),[15] in accord with PST. However, from the TST perspective, the TS is known to tighten with increasing energy,[10,22−30] and therefore the PST description of open channels, which is appropriate at threshold, gives way with increasing energy to channels whose energy spacings are larger than those of the product rotational levels. At energies where

* To whom correspondence should be addressed: wittig@chem1.usc.edu.

10.1021/jp992575s CCC: $18.00
Published on Web 10/07/1999

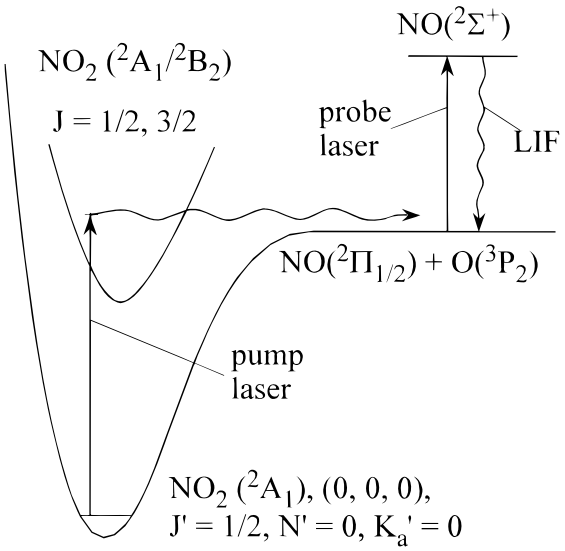

Figure 1. Excitation scheme. A pump pulse whose duration is approximately 20 ps excites NO_2 molecules above the dissociation threshold. After a set delay, a probe pulse whose duration is approximately 20 ps measures the relative amount of NO product via LIF.

tightening is first encountered, the open channels may be described as hindered rotors, but at higher energies they are more like bending levels. This has been discussed by Katagiri and Kato for the case of the NO_2 threshold region.[9]

It is difficult to quantify the tightening of the TS in the threshold regime of a barrierless unimolecular reaction. As mentioned earlier, calculations that use a single PES[10,31,32] provide mechanistic insight but are not suitable for handling long-range interactions. Specifically, the energy region where only the first open channel is available will be associated with a level density that resembles closely the level density just below D_0. This level density has been found to be "anomalously" high compared to an extrapolation over the lower bound levels.[15,17,33−36] For example, the anomalous region in NO_2 is restricted to an interval $\sim$15 cm^{-1} below D_0, where it has been shown that ρ_{vibr} reaches 2.7/cm^{-1}, where ρ_{vibr} is the symmetry-sorted (B_2 or A_1) vibronic level density.[35,36] On the other hand, ρ_{vibr} varies smoothly from 0.11/cm^{-1} at 17 500 cm^{-1} to 0.28/cm^{-1} at 23 600 cm^{-1}, which extrapolates to $\rho_{vibr} = 0.37$/cm^{-1} at D_0.[37,38] Thus, there is an order of magnitude difference between the vibronic level density extrapolated from lower energies and the one observed experimentally just below D_0. It is reasonable to assume that the anomalously high level density just below D_0 will persist as the energy is increased to just above D_0. However, it is not a priori clear just how the density of resonances will vary as the energy above D_0 continues to increase.

Pursuant to the above, it would be desirable to obtain $k(E)$ throughout the threshold regime. Deducing reaction rate constants by analyzing line shapes (e.g., of product yield spectra) is questionable because of spectral congestion. This is not necessarily the case for *all* experimental strategies and molecular systems, e.g., in cases such as overtone pumping it is possible to use spectral selectivity to access a subset of the reactive resonances. However, for the case of NO_2 the bright character provided by the zeroth-order $\tilde{A}^2B_2$ state is spread rather democratically throughout the coupled $\tilde{X}^2A_1/\tilde{A}^2B_2$ manifold, and consequently the congestion problem is severe.

The most direct way to measure reaction rate constants is by using the time-resolved pump−probe method. The experimental strategy is shown schematically in Figure 1. The main technical

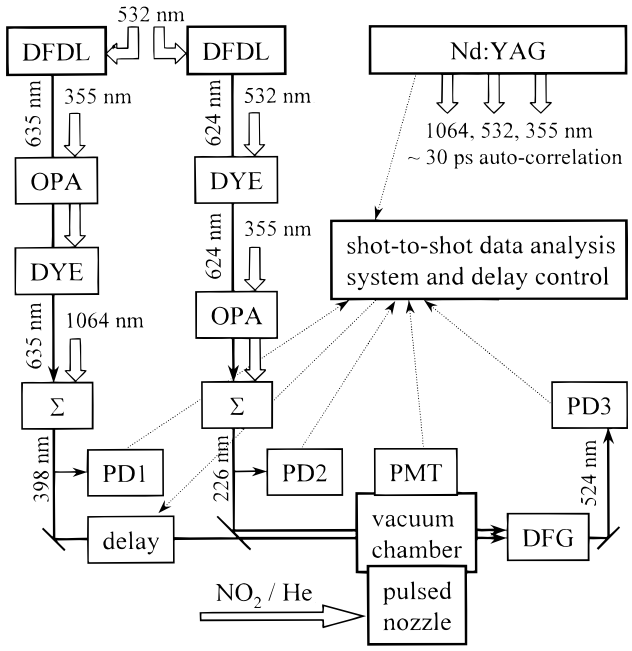

Figure 2. Block diagram of the experimental arrangement. Acronyms not defined in the text are: PD = photodiode; PMT = photomultiplier tube; DFG = difference frequency generation; and Σ = sum frequency generation.

issue is the tradeoff between spectral and temporal resolution. Ultrafast pump−probe systems having cross-correlations of a picosecond or less have spectral widths that are too broad to serve as probes within the lowest open channels. We have carried out pump−probe measurements by using such a source.[21,30,39] The large line widths ($\sim$30 cm^{-1}) result in averaging over several open channels, and consequently the smallest measured rate constants are $\sim 1.6 \times 10^{11}$ s^{-1}, which is substantially larger than what is expected for the first open channel on the basis of spectral measurements, i.e., $\sim 2 \times 10^{10}$ s^{-1}.[15,17]

This order of magnitude difference has prompted us to alter dramatically our pump−probe arrangement, going away from the ultrafast configuration in order to gain some spectral selectivity. This change enables us to establish the missing link between the spectral and time domain studies, both of which have been shown to be highly reproducible. Thus, a marked variation of $k(E)$ is anticipated − an order of magnitude change in just tens of wavenumbers.

The issue of how large a rate constant can be measured in a pump−probe experiment with a given cross-correlation temporal width is subjective. It depends on the signal-to-noise ratio as well as the experience of the group carrying out the measurements. What gets reported also depends on the optimism of those doing the reporting. In the work reported herein, the pump−probe cross-correlation width is $\sim$25 ps and the spectral line width of the pump is $\leq$2 cm^{-1}. We judge that it is possible to measure rate constants with useful accuracy as long as they are smaller than $\sim 10^{11}$ s^{-1}. Though the pump line width spans a number of transitions, resulting in the measurement of an average rate constant,[39] it is smaller than the energy separations between the openings of successive channels, thus enabling the rate variation to be probed as successive channels open.

II. Experimental Section

A block drawing of the experimental arrangement is given in Figure 2. The time-resolved pump−probe technique was used

with ≤20 ps excitation and probe pulses, both having spectral resolution better than 2 cm^{-1}.

A more detailed description of the experimental arrangement will be given elsewhere. Briefly, a new laser setup was employed in which a 30 ps Nd:YAG laser (EXPLA PL 2143C) provided three harmonics (1064, 532, and 355 nm) as optical pump sources. Referring to Figure 2, the pump and probe pulses (having energies up to 100, 50, and 35 mJ at 1064, 532, and 355 nm, respectively) were obtained as follows. The 635 nm output of a temperature stabilized distributed feedback dye laser (LUK DFDL), which was pumped with a fraction of the 532 nm radiation, was first amplified in a BBO optical parametric amplifier (OPA) pumped by ∼10 mJ of 355 nm radiation. The amplified 635 nm radiation was then mixed with ∼50 mJ of the Nd:YAG fundamental in a BBO mixing stage to give the 398 nm pump pulse. The 624 nm output of another DFDL laser was preamplified in a dye cell pumped by a 532 nm pulse, amplified in a BBO OPA pumped by ∼10 mJ of a 355 nm pulse, and mixed with the same 355 nm pulse in another BBO crystal to yield the 226 nm probe pulse. The line width and center frequency of the 226 nm pulse were obtained by recording the laser induced fluorescence (LIF) spectrum of the small amount of NO present as a contaminant in the molecular beam.

Rotationally cold NO_2 was prepared by using supersonic expansion of ∼0.5% NO_2 (Matheson 99.5%) in helium at ∼5 atm through a 0.5 mm nozzle into an evacuated chamber. This is known to populate predominantly the two lowest rotational states.[16] The NO_2 was then excited by a pump pulse at ∼398 nm and NO product was monitored by using LIF, with the ∼226 nm probe pulse set at the 0−0 R_{11} line of the $A^2\Sigma^+ \leftarrow X^2\Pi_{1/2}$ system. The LIF yield was recorded as a function of pump−probe delay, which was varied by using a computer-controlled delay stage (Aerotech ATS150−250).

The rotational temperature (T_R) of the expansion-cooled NO_2 has not been measured directly. However, the expansion conditions are known to lead to a T_R of ∼2 K, in which case only the two lowest rotational levels have significant population.[16] This was confirmed by recording an NO LIF yield spectrum with a large pump−probe delay. This spectrum is similar to the one reported by Butenhoff and Rohlfing,[14] though individual spectral features cannot be resolved with our line width. The abrupt rise of the yield spectrum at 25 126 cm^{-1} is due to NO_2 excited from its second rotational level.

The frequency measurements of the pump pulse were made with a wavemeter (Burleigh WA-4500) calibrated against a multimode HeNe laser. The pump laser frequency and line width were outside the wavemeter's high-performance operation range, so absolute calibration was improved by using the NO LIF yield spectrum. Namely, the middle of the abrupt rise of the yield spectrum was taken to be 25 126 cm^{-1}, and a systematic correction of 1 cm^{-1} was added to the wavemeter's readings. Calibration accuracy is believed to be ±1 cm^{-1}.

The main experimental obstacle was frequency drift of the DFDL lasers, which is probably due to the active temperature stabilization of the dye cell. We estimate the amplitude of temperature oscillations to be ∼0.1 K, which corresponds to frequency oscillations of ∼0.5 cm^{-1}. Though smaller than the excitation laser line width, these oscillations of the probe frequency could impose a spurious time dependence on the LIF signals as the probe frequency goes in and out of resonance. This effect can be reduced by averaging scans taken under the same conditions.

Pump−probe cross-correlations were recorded simultaneously with the signals by generating a difference frequency (524 nm) in a 5 mm long BBO crystal. The measured cross-correlations were used in the fitting routines, which are described elsewhere.[39]

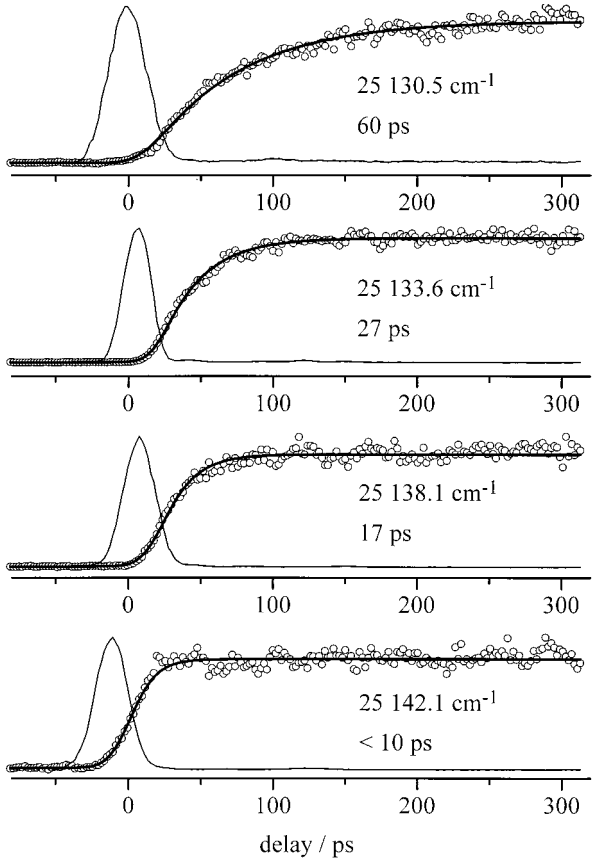

Figure 3. Examples of experimental data (circles), cross-correlations (bell shaped thin lines), and fits to the data assuming a single-exponential rise (thick lines). Values of $\langle h\nu \rangle$ and the buildup times are given underneath each trace. Note the rapid increase of the rate. Traces with buildup times less than ∼10 ps cannot be fit with good reliability.

The main improvement to the data acquisition system was the ability to record signal, cross-correlation, and pump and probe pulse energies on a shot-to-shot basis. This allowed better data handling after the experiment. Signals and cross-correlations could then be normalized to the pulse energies, saturation studies could be conducted, etc.

III. Results

Approximately 50 traces of product LIF buildup have been recorded for $\langle h\nu \rangle$ values ranging from approximately 2.5 cm^{-1} below D_0 to approximately 17 cm^{-1} above D_0, where $\langle h\nu \rangle$ denotes an average over the pump laser line width. Each trace consists of 4 to 20 scans. Each scan has been fit to a single exponential buildup, which constitutes a measurement of the average dissociation rate.[39] The most striking feature is that the rate constant changes by an order of magnitude throughout this rather modest energy range. Figure 3 gives examples of the buildup traces, the corresponding pump−probe cross-correlations, and the fits obtained by assuming single-exponential product buildup. The four $\langle h\nu \rangle$ values used in the figure display buildup times ranging from 60 ps (top) to less than 10 ps (bottom).

Figure 4 gives a summary of all of the results obtained to date. Each point is averaged over a number of scans, and data taken at energies within 1 cm^{-1} of one another have been

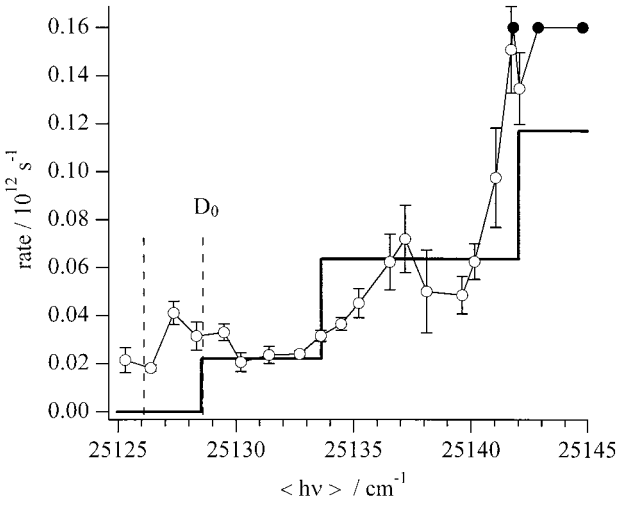

Figure 4. Dissociation rates of rotationally cold NO_2 as a function of $\langle h\nu \rangle$. Open circles: experimental data; error bars represent standard deviations. The solid circles represent traces whose rise times are too short to enable reliable values of the rates to be obtained. Thick solid line: PST calculation for NO_2 excited from the lowest rotational level. The two dashed lines are reaction thresholds for NO_2 starting in its lowest rotational level (i.e., D_0) and its first excited rotational level.

averaged together. The horizontal axis is only accurate to ± 1 cm^{-1}, because of the calibration method described in section II. Note the data points at $\langle h\nu \rangle < D_0$. They reflect both the threshold for the first excited NO_2 rotational level (25 126 cm^{-1}), whose population is comparable to that of the lowest rotational level,[14,16] as well as the spectral width of the pump pulse, which is ≤ 2 cm^{-1}. As $\langle h\nu \rangle$ increases, there is, on average, an increase in the rate constant, though the k versus E variation appears to be nonmonotonic. Work in progress will yield higher quality data and a more accurate determination of $k(E)$. One thing is certain, an abrupt step is not observed at the energy where the second channel is expected to open. Specifically, PST predicts an abrupt step at $D_0 + 5$ cm^{-1} when NO_2 is photoexcited from its lowest rotational level (see Figure 4).

At approximately 25 141 cm^{-1}, the rate constants increase substantially — so much so that some of them cannot be measured by using the present configuration. The lower bound for the three black points in Figure 4 is $\sim 10^{11}$ s^{-1}. They are placed in the figure at the value 1.6×10^{11} s^{-1} (without error bars), in accord with previous measurements,[21,30,39] with the understanding that this is a rough lower bound. The abrupt increase in $k(E)$ is unmistakable, as is also clear from Figure 3.

In our earlier measurements, in which line widths of ~ 30 cm^{-1} were used,[21,30,39] the average rate constant in this region was found to be 1.6×10^{11} s^{-1}. Thus, given the relatively small rate constants observed at excess energies up to ~ 14 cm^{-1} in the present study, it was inevitable that $k(E)$ would increase markedly near this point. Otherwise the earlier rate constant measurements (which were averaged over line widths of ~ 30 cm^{-1}) would not have consistently yielded such high values.

Referring to Figure 4, the thick solid staircase curve superimposed on the data is a PST calculation of the rate constant, assuming that NO_2 starts in its lowest rotational level, and using a symmetry-sorted vibronic level density of 2.7/cm^{-1}, i.e., the vibronic level density that has been measured just below D_0.[35,36] Details are given in the Appendix. The PST calculation fails to predict both the abrupt rise in $k(E)$ at the energy where the second channel opens, as well as the large increase observed at ~ 14 cm^{-1}.

IV. Discussion

It has been concluded from the vast number of experiments and calculations carried out during the past decade that NO_2 decomposes via a unimolecular reaction mechanism throughout an energy regime that starts at threshold (i.e., D_0 for nonrotating molecules) and extends to many thousands of wavenumbers.[10,18,20,31] This system has served as an excellent prototype, illustrating important features of models which are used to describe barrierless unimolecular reactions — from the classic work of Mies and Krauss dealing with overlapping resonances and the corresponding quantum fluctuation phenomena[40,41] to standard statistical theories such as PST and RRKM, in which quantum fluctuation phenomena are not present.

The threshold regime of a barrierless unimolecular reaction yielding radical fragments is subtle, and effects due to quantum fluctuations and long-range interactions are expected to be prominent. For example, fluctuation phenomena are anticipated for observables such as product state distributions (PSDs), rate constants, correlations, laboratory and molecular frame anisotropies, etc. Indeed, with NO_2 this has proven to be the case.[18]

However, *very* near threshold, within the first few open channels, the situation is more complex than simply one of quantum fluctuations on a single PES. Multiple PESs and the couplings between them must be considered on an equal footing with the couplings to the continua, because all PESs that correlate to the same products are degenerate at large interfragment distances, even if they are repulsive at shorter distances. Thus, just above threshold it is imprudent to ignore the participation of excited PESs in favor of just the ground PES or, in the case of NO_2, the mixed $\tilde{X}^2A_1/\tilde{A}^2B_2$ system. This has been discussed by Graff and Wagner,[42] who have used a semiempirical method to obtain the long-range potentials for $OH(^2\Pi_{1/2,3/2}) + O(^3P_{2,1,0})$, a system which is very similar to the $NO(^2\Pi_{1/2,3/2}) + O(^3P_{2,1,0})$ system under consideration here. The long-range potentials thus obtained are of good accuracy. They illustrate how electrostatic-type attraction influences the many PESs that converge asymptotically to the radical products. Large-scale electronic structure calculations have also been carried out for the NO_2 threshold regime with spin−orbit interaction included.[9] Again, one sees the innate complexity and the inevitability of the participation of multiple PESs. The question then arises: How is this complexity manifested in measured properties such as reaction rate constants?

Compelling evidence for the importance of long-range attractive interactions and the possible participation of multiple PESs has been provided by spectra recorded a few wavenumbers below D_0.[33−36] These spectra reveal a dramatic increase in the vibronic level density just below D_0. It is difficult to rationalize this increase without invoking long-range attractive interactions and more than just the mixed $\tilde{X}^2A_1/\tilde{A}^2B_2$ system.

It is an interesting fact that the threshold regime of unimolecular reactions has nearly always been discussed in terms of statistical models. These computational benchmarks are believed to provide credible perspectives in the sense that, with sufficient averaging over fluctuations, the statistical models are recovered. However, this thesis is unproved. For example, the anomalously high level densities observed near D_0 have nothing to do per se with averaging over quantum fluctuations. Yet, they are probably a much more general trait of barrierless unimolecular reactions than has hitherto been recognized. In the threshold region, it would be strange indeed if the system *did* follow PST, variational RRKM, etc. Rather, the observables are expected to be rife with dynamical bias, yet evolve with increasing energy to the regime where statistical theories are appropriate.

It is with the aforementioned issues and caveats in mind that we comment here on the results presented in section III. These data are the natural complement to the host of spectroscopic studies which have been carried out at energies below D_0.[13,14,33−38,43−46] Relatively few spectroscopic studies have been carried out above D_0.[13−18] Though they illustrate the presence of resonances and provide some good qualitative information, they are not well suited for obtaining rate constants, due to severe spectral congestion. Specifically, line width analyses can provide rough estimates of rate constants for the first open channel,[15,17] but thereafter line width (or line shape) analyses are questionable. Rate constants can also be inferred from measurements of laboratory frame anisotropies,[19] but only rough estimates can be obtained with acceptable confidence. Of course, rate constant measurements of the type reported here average over a number of resonances, so widths of individual resonances are not obtained. However, this is not a serious drawback, since there is spectral congestion and consequently some degree of averaging is inevitable, regardless of the resolution.

The main issue to be discussed is the behavior of $k(E)$ in the threshold regime. In the present work, this can be taken to be the first three open channels of PST. Since the samples are rotationally cold, centrifugal effects are minimal, so we can concentrate on issues relating to vibronic levels and long-range interactions.

When the first reactive channel opens, its center-of-mass (c.m.) translational energy is minuscule and its TS is ill-defined. One can say it lies at distances that are so large they are sometimes referred to as infinity. As the energy increases, the TS moves inward. This scenario is repeated following the successive openings of the second, third, etc. channels. Were the system in the PST limit, new channels would open successively at approximately the energies of the NO rotational levels until the higher oxygen and NO spin−orbit levels are encountered. (This assumes minimal cutoff from centrifugal barriers.) One signature of tightening of the TS is that the opening of successive channels occurs at energies that are slightly larger than the energy spacings of the NO rotational levels.

Miyawaki et al.[15] have reported a number of Lorentzian line widths (and the corresponding rate constants) for the first 13 cm^{-1} above D_0 for samples cooled to $T_{rot} \cong 1$ K, in which case NO_2 is predominantly in its lowest rotational level. Compared to the data shown in Figure 4, there are a few differences worth noting, e.g., they report an abrupt increase in the rate constant when the energy is increased to $\sim$6 cm^{-1} above D_0, whereas this is not observed in our measurements. However, the average rate constants in the region of the first open channel are similar for the two data sets, i.e., they are both $\sim 2 \times 10^{10}$ s^{-1}. Likewise, they report that $k(E)$ goes through a maximum at $\sim$8 cm^{-1} above D_0 and then drops until the end of the range they examined (13 cm^{-1}), and we observe the same qualitative behavior. Our results are also consistent with the data of Abel et al.[17] Though it is hard to discern a qualitative change at $D_0 + 5$ cm^{-1} from Figures 10 and 11 of their paper, the average values agree with our measurements.

A significant observation is the marked increase in $k(E)$ at $\sim$25 141 cm^{-1} (Figure 4). This lies just beyond the energy region where Miyawaki et al. carried out line width analyses. Note that the relatively fast rate constants measured for $\langle h\nu \rangle \geq$ 25 141 cm^{-1} cannot be extracted from yield spectra. This increase of $k(E)$ is not predicted by the PST calculation. Within the context of PST, the only way to accommodate such a large increase is by having $\rho(E)$ decrease, an idea that is anathema to conventional theories of unimolecular reactions. However, we deem a decrease of $\rho(E)$ probable, as discussed below.

At long range, where it is known that electrostatic-type interactions are important, couplings between the mixed $\tilde{X}^2A_1/\tilde{A}^2B_2$ vibronic system and other PESs are likely to occur. This results in a bound level density which is higher than at slightly lower energies, where the long-range portions of the surfaces are inaccessible. Just above D_0, it is reasonable to assume that the anomalously high level density observed just below D_0 will persist, at least over some modest energy interval.

As the energy increases and the TS tightens, the TS can move to smaller distances than the region where long-range interactions result in the anomalously high level density. Thus, the level density can actually *drop*. In this case, the unimolecular decomposition rate can increase by a larger amount than is anticipated solely on the basis of the successive opening of reactive channels.

This qualitative picture is acceptable as long as the TS lies at larger distances than the region where the $\tilde{X}^2A_1/\tilde{A}^2B_2$ vibronic system couples to the other PESs. However, when the energy increases and the TS moves inward, the "molecular region" can then lie at shorter distances than the region where the $\tilde{X}^2A_1/\tilde{A}^2B_2$ vibronic system couples to the other PESs. In this case, it is meaningless to include in the "molecular region" effects which are due to long-range interactions that are present at distances beyond the TS. This is a qualitative rationalization of the data in Figure 4 in terms of a drop in the level density. It is an *interpretation* from a TST perspective. However, the bottom line is that the rate constant displays a prominent increase with energy. The observed $k(E)$ variation, though somewhat erratic and not of the highest possible experimental accuracy, suggests that the dynamics are complicated.

Finally, we note that the present results are surprisingly consistent with the ab initio calculations of Katagiri and Kato.[9] Their Figure 9 shows adiabatic bending potential curves, built on ground and electronically excited PESs, which have shallow attractive regions at O−NO distances greater than 4 Å. This can account for the anomalous level density. Moreover, the first and second open channels have barrierless adiabatic curves, suggesting TSs at large distances along the reaction coordinate. The adiabatic bend which is correlated to the third NO rotational level has a barrier at $\sim$3 Å, indicating that the TS tightens to this distance at an energy between the second and third . Once it tightens, the region $\sim$4 Å which gives rise to the additional density of states due to electronic mixing lies on the product side. The level density drops to the normal value of $\sim 0.4/cm^{-1}$ and the rate increases. The third channel opens as soon as the energy exceeds $\sim$80 cm^{-1} above D_0, in accord with the experimental observations of Ionov et al.[30] This explanation, while speculative, is amusing in the sense that the agreement is better than one has a right to expect.

At energies below $\sim$25 141 cm^{-1}, i.e., the energy where $k(E)$ rises abruptly, there appear to be local minima in k versus E, based on both the present measurements and the line width analysis of Miyawaki et al. This needs to be proved by more accurate measurements. If this variation is confirmed, it will not be possible to rationalize this effect by using a simple statistical theory. Again, this result would underscore the need to consider near-threshold dynamical processes directly, without undue reliance on a statistical perspective.

The work presented above illustrates some of the complexity and subtleties associated with the threshold regime. For reactions that take place at temperatures of several hundred K or higher, the details about the threshold regime discussed in this paper

are not important insofar as rates are concerned. On the other hand, for low-temperature interactions, such details are very important and may change the way such processes are thought about.

Acknowledgment. This research was supported by the U.S. Department of Energy under contract no. DE-FG03-85ER13363. The authors have benefited from discussions concerning this work with numerous scientists, including H. Reisler, B. Cao, S. Grebenshchikov, B. Abel, A. Delon, and P. Itskowitz.

Appendix

PST can be applied straightforwardly to the $O(^3P_2) + NO(X^2\Pi_{1/2}, v = 0)$ products. The higher spin−orbit states, i.e., $O(^3P_{1,0})$ and $NO(X^2\Pi_{3/2})$, are not energetically accessible in the present study. Here we consider photoexcitation of NO_2 molecules having $J_{NO_2} = 1/2$, in which case photoexcitation prepares $J_{NO_2} = 1/2$ and 3/2. Since rotational excitation is minimal, centrifugal effects are assumed to be negligible, and levels are counted up to the limits imposed by energy and angular momentum conservation.

Consider first the case when NO is in its lowest rotational level, i.e., $J_{NO} = 1/2$. Combining $J_O = 2$ and $J_{NO} = 1/2$ yields intermediate J' values of 5/2 and 3/2. Now consider $J_{NO_2} = 1/2$. Adding $\vec{J}' + \vec{L}$ to give a resultant whose magnitude is 1/2 (i.e., $J_{NO_2} = 1/2$) yields $L = 3$ and 2 for $J' = 5/2$, and $L = 2$ and 1 for $J' = 3/2$. Thus, there are four nondegenerate open channels for the lowest NO rotational level. We say that the first open channel (i.e., corresponding to the lowest NO rotational level) has a degeneracy of 4. Now consider $J_{NO_2} = 3/2$. Adding $\vec{J}' + \vec{L}$ to give a resultant whose magnitude is 3/2 yields $L = 4$, 3, 2, and 1 for $J' = 5/2$, and $L = 3$, 2, 1, and 0 for $J' = 3/2$. The degeneracy is 8.

For the second open channel $J_{NO} = 3/2$ and the J' values are 7/2, 5/2, 3/2, and 1/2. For $J_{NO_2} = 1/2$, this yields $L = 4$ and 3 for $J' = 7/2$; $L = 3$ and 2 for $J' = 5/2$; $L = 2$ and 1 for $J' = 3/2$; and $L = 1$ and 0 for $J' = 1/2$. The degeneracy is 8. For $J_{NO_2} = 3/2$, we have $L = 5$, 4, 3, and 2 for $J' = 7/2$; $L = 4$, 3, 2, and 1 for $J' = 5/2$; $L = 3$, 2, 1, and 0 for $J' = 3/2$; and $L = 2$ and 1 for $J' = 1/2$. The degeneracy is 14.

For the third open channel $J_{NO} = 5/2$ and the J' values are 9/2, 7/2, 5/2, 3/2, and 1/2. For $J_{NO_2} = 1/2$ this yields $L = 5$ and 4 for $J' = 9/2$; $L = 4$ and 3 for $J' = 7/2$; $L = 3$ and 2 for $J' = 5/2$; $L = 2$ and 1 for $J' = 3/2$; and $L = 1$ and 0 for $J' = 1/2$. The degeneracy is 10. For $J_{NO_2} = 3/2$ we have $L = 6$, 5, 4, and 3 for $J' = 9/2$; $L = 5$, 4, 3, and 2 for $J' = 7/2$; $L = 4$, 3, 2, and 1 for $J' = 5/2$; $L = 3$, 2, 1, and 0 for $J' = 3/2$; and $L = 2$ and 1 for $J' = 1/2$. The degeneracy is 18. And so it goes for additional open channels. For $J_{NO} \geq 7/2$, the degeneracies for $J_{NO_2} = 1/2$ and 3/2 are 10 and 20, respectively. The counts presented above are easily visualized by using diagrams.[20] Note that NO Λ-doublets are automatically included in the above counting.

The rates are given by $W/h\rho$, where W includes the degeneracies.[1] For example, for the first three open channels with $J_{NO_2} = 3/2$, $W = 8 + 14 + 18 = 40$. For complete K_a breakdown and including spin−rotation interaction, ρ is given by $(2J_{NO_2} + 1)\rho_{vibr}$. Note that the number of open channels is not multiplied by a factor of 2 to account for the identical oxygens. Instead, symmetry sorted ρ_{vibr} is used in the denominator.

References and Notes

(1) Baer, T.; Hase, W. L. *Unimolecular Reaction Dynamics: Theory and Experiments*; Oxford University Press: New York, 1996.
(2) Schinke, R.; Beck, C.; Grebenshchikov, S. Y.; Keller, H.-M. *Ber. Bunsen-Ges. Phys. Chem.* **1998**, *102*, 593.
(3) Mandelshtam, V. A.; Grozdanov, T. P.; Taylor, H. S. *J. Chem. Phys.* **1995**, *103*, 10074.
(4) Salzgeber, R. F.; Mandelshtam, V. A.; Schlier, C.; Taylor, H. S. *J. Chem. Phys.* **1999**, *110*, 3756.
(5) Salzgeber, R. F.; Mandelshtam, V. A.; Schlier, C.; Taylor, H. S. *J. Chem. Phys.* **1999**, *109*, 937.
(6) Skokov, S.; Bowman, J. M.; Mandelshtam, V. A. *Phys. Chem. Chem. Phys.* **1999**, *1*, 1279.
(7) Harding, L. B.; Stark, H.; Troe, J.; Ushakov, V. G. *Phys. Chem. Chem. Phys.* **1999**, *1*, 63.
(8) Leonardi, E.; Petrongolo, C.; Hirsch, G.; Buenker, R. J. *J. Chem. Phys.* **1996**, *105*, 9051.
(9) Katagiri, H.; Kato, S. *J. Chem. Phys.* **1993**, *99*, 8805.
(10) Grebenshchikov, S. Y.; Beck, C.; Flöthmann, H.; Schinke, R.; Kato, S. *J. Chem. Phys.* **1999**, *111*, 619.
(11) Brody, T. A.; Flores, J.; French, J. B.; Mello, P. A.; Pandey, A.; Wong, S. S. M. *Rev. Mod. Phys.* **1981**, *53*, 385.
(12) Mehta, M. L. *Random Matrices*; Academic Press: San Diego, 1991.
(13) Butenhoff, T. J.; Rohlfing, E. *J. Chem. Phys.* **1993**, *98*, 5460.
(14) Butenhoff, T. J.; Rohlfing, E. *J. Chem. Phys.* **1993**, *98*, 5469.
(15) Miyawaki, J.; Yamanouchi, K.; Tsuchiya, S. *J. Chem. Phys.* **1993**, *99*, 254.
(16) Robra, U.; Zacharias, H.; Welge, K. H. *Z. Phys. D* **1990**, *16*, 175.
(17) Abel, B.; Hamann, H. H.; Lange, N. *Faraday Discuss.* **1995**, *102*, 147.
(18) Reid, S. A.; Reisler, H. *J. Phys. Chem.* **1996**, *100*, 474.
(19) Demyanenko, A. V.; Dribinski, V.; Reisler, H.; Meyer, H.; Qian, C. X. W. *J. Chem. Phys.* **1999**, in press.
(20) Hunter, M.; Reid, S. A.; Robie, D. C.; Reisler, H. *J. Chem. Phys.* **1993**, *99*, 1093.
(21) Ionov, P. I.; Bezel, I.; Ionov, S. I.; Wittig, C. *Chem. Phys. Lett.* **1997**, *272*, 257.
(22) Klippenstein, S. J.; Khundkar, L. R.; Zewail, A. H.; Marcus, R. A. *J. Chem. Phys.* **1988**, *89*, 4761.
(23) Klippenstein, S. J.; Marcus, R. A. *J. Chem. Phys.* **1989**, *91*, 2280.
(24) Klippenstein, S. J.; Marcus, R. A. *J. Chem. Phys.* **1990**, *93*, 2418.
(25) Klippenstein, S. J.; East, A. L. L.; Allen, W. D. *J. Chem. Phys.* **1996**, *105*, 118.
(26) Marcus, R. A. *J. Chem. Phys.* **1986**, *85*, 5035.
(27) Marcus, R. A. *Chem. Phys. Lett.* **1988**, *144*, 208.
(28) Miller, W. H. *J. Chem. Phys.* **1976**, *65*, 2216.
(29) Wade, E. A.; Mellinger, A.; Hall, M. A.; Moore, C. B. *J. Phys. Chem. A* **1997**, *101*, 6568.
(30) Ionov, S. I.; Brucker, G. A.; Jaques, C.; Chen, Y.; Wittig, C. *J. Chem. Phys.* **1993**, *99*, 3420.
(31) Klippenstein, S. J.; Radivoyevitch, T. *J. Chem. Phys.* **1993**, *99*, 3644.
(32) Troe, J. *J. Chem. Phys.* **1983**, *79*, 6017.
(33) Miyawaki, J.; Yamanouchi, K.; Tsuchiya, S. *J. Chem. Phys.* **1994**, *101*, 4505.
(34) Ionov, S. I.; Davis, H. F.; Mikhaylichenko, E.; Valachovic, L.; Beaudet, R. A.; Wittig, C. *J. Chem. Phys.* **1994**, *101*, 4809.
(35) Jost, R.; Nygård, J.; Pasinski, A.; Delon, A. *J. Chem. Phys.* **1996**, *105*, 1287.
(36) Delon, A.; Heilliette, S.; Jost, R. *Chem. Phys.* **1998**, *238*, 465.
(37) Georges, R.; Delon, A.; Jost, R. *J. Chem. Phys.* **1995**, *103*, 1732.
(38) Delon, A.; Jost, R.; Lombardi, M. *J. Chem. Phys.* **1991**, *95*, 5701.
(39) Bezel, I.; Ionov, P.; Wittig, C. *J. Chem. Phys.* **1999**, in press.
(40) Mies, F. H.; Krauss, M. *J. Chem. Phys.* **1966**, *45*, 4455.
(41) Mies, F. H. *Phys. Rev.* **1968**, *175*, 164.
(42) Graff, M. M.; Wagner, A. F. *J. Chem. Phys.* **1990**, *92*, 2423.
(43) Delon, A.; Jost, R. *J. Chem. Phys.* **1991**, *95*, 5686.
(44) Delon, A.; Dupre, P.; Jost, R. *J. Chem. Phys.* **1993**, *99*, 9482.
(45) Delon, A.; Georges, R.; Jost, R. *J. Chem. Phys.* **1995**, *103*, 7740.
(46) Georges, R.; Delon, A.; Bylicki, F.; Jost, R.; Campargue, A.; Charvat, A.; Chenevier, M.; Stoeckel, F. *Chem. Phys.* **1995**, *190*, 207.